Engineering Fracture Mechanics 297 (2024) 109880

Contents lists available at ScienceDirect

Engineering Fracture Mechanics

journal homepage: www.elsevier.com/locate/engfracmech

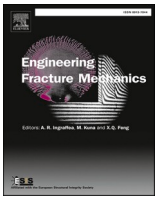

Evaluating the impact of calcite and heterogeneity on the mechanical behavior of coal: A numerical study with grain-based finite-discrete element method

Sajid Ali [a], Chengzeng Yan [a,b,c,*], Tie Wang [a], Yuchen Zheng [a], Du Han [a], Wenhui Ke [d]

[a] Faculty of Engineering, China University of Geosciences, Wuhan, China
[b] State Key Laboratory of Intelligent Construction and Healthy Operation and Maintenance of Deep Underground Engineering
[c] National Center for International Research on Deep Earth Drilling and Resource Development, China University of Geosciences, Wuhan 430074, China
[d] Wuhan Municipal Construction Group Co., Ltd., Wuhan, Hubei 430023, China

ARTICLE INFO

Keywords:
Coal: Calcite
Heterogeneity
Grain-based model
Finite-discrete element method
MultiFracS

ABSTRACT

Understanding the mechanical properties and fracture behaviors of coal is essential for the safety of underground mining engineering. This research aims to evaluate the impact of calcite and heterogeneity on the mechanical properties of coal. Neper, a software package for polycrystal generation and meshing, is used to create numerical models with a non-uniform grain size distribution. A random parameter assignment method is proposed to simulate the mechanical properties and failure behavior of coal using the combined finite-discrete element method (FDEM). A comprehensive parametric investigation of the properties of triangular and joint elements is conducted, and calibration procedures are suggested for numerical modeling. The model was calibrated to experimental results and then used to understand the impact of calcite grains on the mechanical behavior of coal. After calibration, a triaxial compression was performed on coal samples with and without calcite grains at different confining pressures. It is found that the presence of calcite in a coal sample increases Young's modulus and decreases the peak strength of coal. This research uses Voronoi tessellation technology to present a Weibull statistical grain-based model (GBM) to investigate the microstructural heterogeneity induced by grain morphologies. The deformation response, strength characteristics and cracking behavior are investigated by varying the heterogeneity of numerical models under compressive tests with different confining pressures. The simulation results of triaxial compression indicate that the compressive strength increases linearly as the heterogeneity m value increases. The consistency of the numerical results with the experimental observations suggests that the GBM approach can be used to better understand the mechanics of brittle rock failure at the micro-structure scale.

1. Introduction

A comprehensive and accurate understanding of the mechanical properties of coal under the confining pressure effect can provide a certain theoretical basis and practical value for controlling the stability of underground mines [1–5]. Considerable research has been

* Corresponding author at: Faculty of Engineering, China University of Geosciences, Wuhan, China.
E-mail address: yancz@cug.edu.cn (C. Yan).

https://doi.org/10.1016/j.engfracmech.2024.109880
Received 18 August 2023; Received in revised form 9 January 2024; Accepted 14 January 2024
Available online 17 January 2024

done to investigate the mechanical properties of coal under the influence of confining pressure, and numerous researchers have obtained abundant research achievements, particularly in the fields of loading methods, loading stress directions and research perspectives. Limited literature is available regarding the influence of confining pressure on the mechanical properties of coal. Therefore, it is necessary to analyze the effect of confining pressure on the mechanical properties of coal.

Minerals found within coal formations are heterogeneous in nature and depend upon several factors, such as source rocks, lithology, weathering rate, hydrology and the degree of coalification [6]. The prominent minerals found in coal are quartz, illite, pyrite, rutile and calcite. The mineral composition of coal has significant importance in several aspects, ranging from its extraction to its utilization. Many studies have investigated the effects of the mineral composition and microstructure of coal on different aspects, such as the design and selection of drilling fluids for the extraction of coal bed methane [7], CO2 sorption [8,9], human health and cleaning procedure of coal [10–12].

Generally, rock consists of different minerals, pores, cracks, joints and layering, and hence, the heterogeneities of these geomaterials are distinct. It is necessary to understand that all rocks have inherent heterogeneity [13]. Compared to the homogenous assumption of rock, the heterogeneity of rock, including mineralogical composition, grain shape, grain packing and contact between grains, directly affects its mechanical properties [14]. Therefore, it is necessary to study the effect of rock heterogeneity on its strength and failure mechanism.

Many researchers have studied the influence of heterogeneity on the failure behavior and strength of rock [15–22]. The key issue is to characterize heterogeneity to obtain their corresponding parameters. The development of micrometer-scale evaluation technology has played a significant role in implementing digital image processing (DIP) technique for determining material microstructures and the spatial distribution of minerals [23,24]. Various numerical simulation methods combined with digital image processing (DIP) technology have been used to investigate the heterogeneous properties of rock materials. The most common methods are the FEM [25], FDM [16,26], DEM [14] and FDEM [18]. DIP technique can simulate rock's actual geometric heterogeneity and microstructures in numerical modeling. However, this technique still has certain limitations.

Therefore, indirect or equivalent approaches to describe rock heterogeneity have been proposed consecutively, including the grain-based model (GBM) [21] or its extended model [22] and the random parameter assignment method [27,28]. In the GBM model, a mineral grain is often used as a Voronoi block, filled with smaller elements. However, the Voronoi block shows a degree of consistency and similarity [29] to its shape and size compared to real mineral grains, which include irregular shapes and uneven sizes [22]. The importance of Voronoi block shape and size in numerical modeling cannot be ignored when considering the failure behavior of rock samples [17,20,30,31]. To minimize the influences shape and size of Voronoi block, the block must be sufficiently meshed to a small enough size, which reduces computation efficiency, making engineering scale simulation challenging. Therefore, the GBM method mainly simulates the mechanical and failure characteristics of heterogeneous rock samples at laboratory scale, such as uniaxial compression [32–34], triaxial compression [30], Brazilian disc [35,36] and direct shear [29].

With the continuous development in computing technology, numerical modeling has become a valuable and optimal solution to resolve these challenges. Two distinct categories can be used to represent ongoing strategies for generating heterogeneity in calculation models [37]: (a) continuum methods and (b) discontinuum methods. The basic idea of continuum methods is to discretize complex models and transform the displacement and stress fields into linear or nonlinear equations to solve [38], which is favorable for modeling engineering problems [39–42]. However, continuous methods cannot deal with complex discontinuities and capture microscopic damage and failure behavior because the geomaterials would break during loading. Therefore, other numerical methods to deal with discontinuities have been developed, such as discrete element method [36,43], Particle Flow Code [16,44] and discontinuous deformation analysis [45].

Compared to the continuum and discontinuum methods, FDEM has recently gained importance in geotechnical and underground space engineering due to its ability to simulate the transition from continuous to discontinuous solid states. Many scholars have contributed significantly by implementing numerous novel features to the fundamental mechanical framework of the FDEM [46–53]. Particularly, Yan et al. proposed the adaptive finite-discrete element method [54] and built many FDEM based THM coupled models [55–82]; all of these models have been integrated into the MultiFracS software [54,65,83], which significantly improves the application scope of FDEM. Therefore, this study introduces the Weibull distribution function in the FDEM-GBM model to investigate the microstructural heterogeneity caused by grain morphologies using Voronoi tessellation technology.

This study investigated the impact of calcite grains on the mechanical behavior of coal. A grain-breakable FDEM model was constructed based on the mineral composition data of the coal containing calcite grains. The model was calibrated to experimental results, and then triaxial compression tests with different confining pressures were conducted to understand the effect of calcite grains on the mechanical behavior of coal. A Voronoi tessellation technique coupled with a Weibull distribution is used and implemented in MultiFracS to simulate the heterogeneity of the real microstructure of coal with calcite grains. The rock strength, deformation behavior, and associated crack initiation and propagation of numerical models are investigated and discussed by executing numerical tests on specimens with different homogeneity indices.

2. Model and methodology

2.1. A brief introduction to FDEM and Neper

The FDEM was initially conceived by Munjiza [49,84–86], which is particularly suitable for simulating solid fracture due to its special element topological connection. The fundamental principle of this method is that the continuum is discretized into finite triangular element mesh, and the initial joint element with no thickness is implemented across the common edge of adjacent triangular

elements to create a cohesive effect, then each triangular element does not share a node Fig. 1(a). The simulation of crack initiation, propagation, and intersection is accomplished by the broken of joint elements. The triangular element is a kind of constant strain element that shares the continuous deformation with the unbroken joint element. Fracture constitutive models for joint elements can be categorized into three types; namely model I, model II and model I-II, define the failure modes of tensile, shear and mixed tensile-shear, respectively as illustrated in Fig. 1(b). There are numerous research on the detailed basic principles of FDEM [49,50,57,85,87].

2.2. Governing equation in FDEM

The system dynamic equation implemented in the FDEM is similar to the DEM equation, which is solved using Newton's second law:

$$M\ddot{x} + C\dot{x} = F(x) \tag{1}$$

where:

M represents the mass matrix.

C repents the damping matrix.

$F(x)$ is the node unbalanced vector. This vector represents many forces, including the contact force F_c, the node force F_d resulting

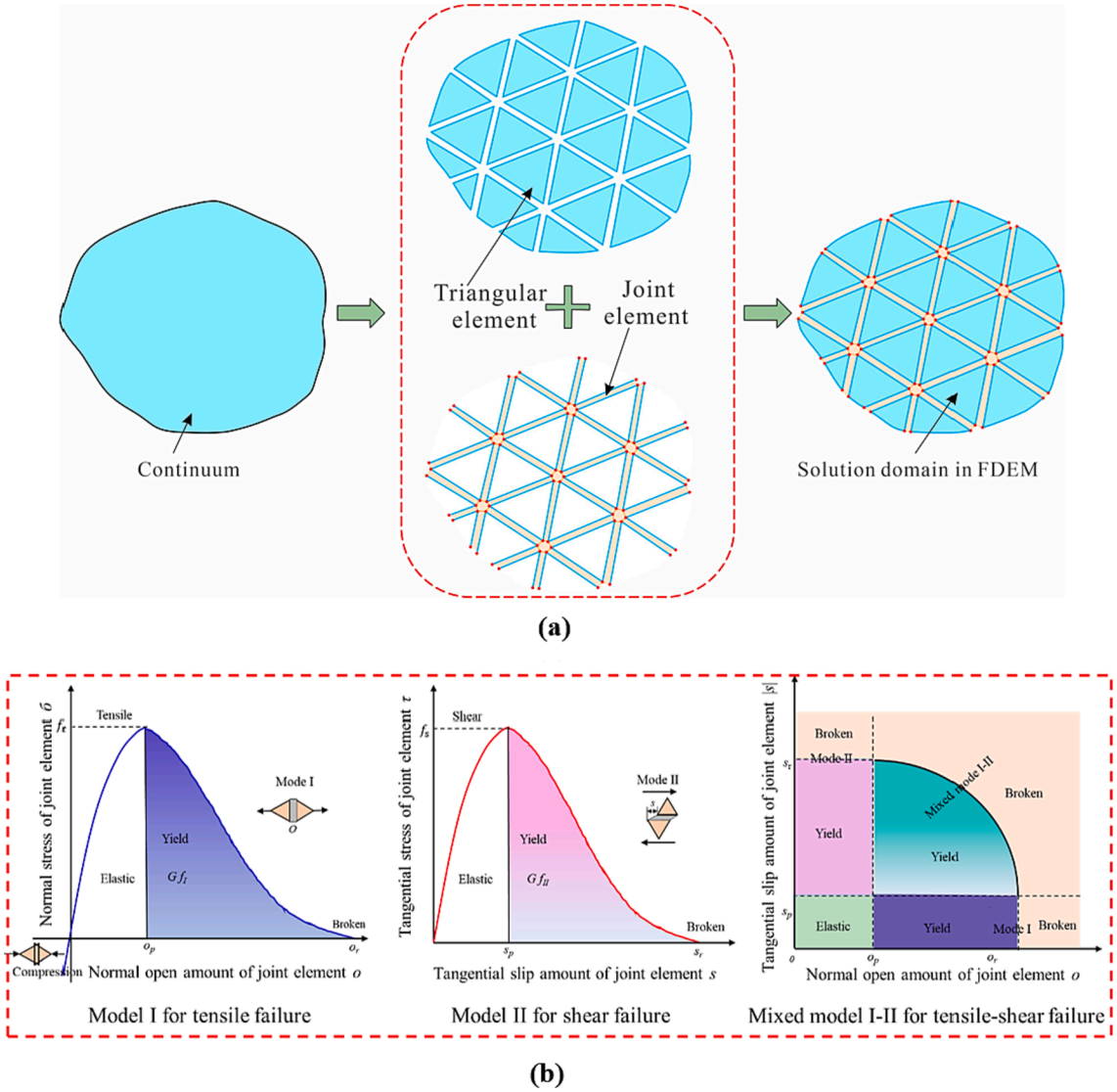

Fig. 1. Basic ideas of FDEM (a) the solution of continuum and connection relationship between triangular and joint elements (b) three types of fracture constitutive models of the joint element after Munjiza et al. [85].

from the deformation of the triangular element, the node force F_e obtained from the external loading and the node force F_j developing from the cohesive force of the joint elements.

2.3. Deformation and stress of the triangular element

The FEM calculates the deformation and stress characteristics of the triangular element. The constitutive relation for isotropic elements is expressed as follows [86]:

$$T = \frac{1}{\sqrt{|\det \mathbf{F}|}}\left[\frac{E}{1+\upsilon}\mathbf{E}_d + \frac{E}{1-\upsilon}\mathrm{E}_s + 2\mu\mathbf{D}\right] \tag{2}$$

where:

T represents the tensor stress in a whole coordinate system after finite element deformation.
$\mathbf{F}$ denotes the deformation gradient.
$\mathbf{E}_d$ is the Gree-St Venant strain tensor due to shape modifications.
E_s represents the Gree-St Venant strain tensor due to shape change.
υ represents the Poisson's ratio of the material.
μ is the damping coefficient.
$\mathbf{D}$ is the strain rate tensor.

2.4. Contact detection and contact force

FDEM employs the efficient non-binary search (NBS) contact detection algorithm [88] for contact detection and adopts a potential-based strategy [89] for evaluating contact force. The time-consuming NBS contact detection algorithm is linear with element numbers. The potential-based contact force calculation method overcomes the difficulty of traditional DEM in dealing with point-point contact because of its distributed contact force.

The finite element mesh of the triangular element discretizes the continuum in the solution domain in FDEM, allowing the triangular element to solve the contact force of the blocks. The example in Fig. 2(a) illustrates two triangles in contact. These triangles are generally called the contactor triangle β_c and the target triangle β_t. The contact force throughout the whole overlapping domain is equal to the force transmitted from β_c to β_t, which is followed by the force produced from β_t to β_c in the opposite direction. The overall contact force within the overlapping domain is [86,89]:

$$f_c = p_n \int_{\Gamma\beta_c \cap \beta_t} [grad\varphi_c(P_c) - grad\varphi_t(P_t)]dA = p_n \oint_{\Gamma\beta_c \cap \beta_t} n_\Gamma(\varphi_c - \varphi_t)d\Gamma \tag{3}$$

where:

p_n denotes the normal penalty.
grad represents gradient.

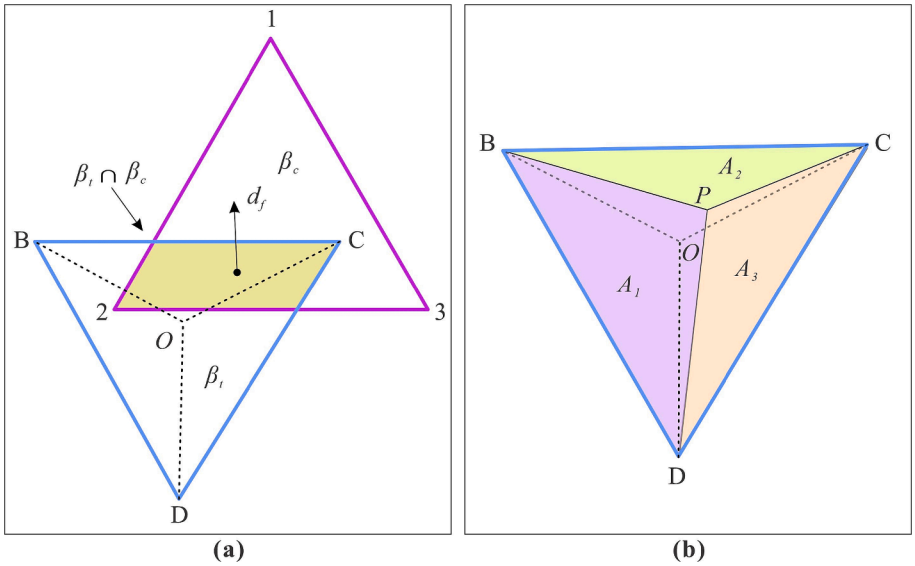

Fig. 2. (a) Solution of the contact force between triangular elements and (b) potential of any point inside the triangular element.

A is the overlapping area.
P_c represents an overlapping point in β_c.
P_t is an overlapping point in β_t.
$\varphi_c(P_c)$ is the potential of P_c in β_c.
$\varphi_t(P_t)$ is the potential of P_t in β_t.
n_Γ represents the outer normal vector of the overlapping area.
$\Gamma\beta_c \cap \beta_t$ represents the boundary of two triangles in overlapping areas.

In addition to developing the meaning of the potential function φ, the potential-based contact force needs to fulfill specific criteria. The potential function must keep constant throughout the boundary of the element. Furthermore, the work done by the contact force must be equal to 0 under these circumstances. For this study, the potential function given by Munjiza [86] is as follows:

$$\varphi(P) = \min\left\{\frac{3A_1}{A}, \frac{3A_2}{A}, \frac{3A_3}{A}\right\} \tag{4}$$

where:
A represents the area of the triangular element.
A_1, A_2 and A_3 are the sub-triangle areas comprised of point P and three sides of the triangle, as illustrated in Fig. 2(b).

2.5. The Neper software

Neper is a robust open-source package for polycrystal generation and meshing in 2D and 3D [90]. It can be compiled and run on any Unix-like operating system. The program consists of three main modules: generation, meshing, and visualization. Neper generates polycrystals as Voronoi tessellations with convex-shaped cells in a space domain (i.e., cuboidal, cylindrical and spherical-shaped domains). There are two ways to generate tessellations: one is from cell morphological properties, such as grain size distribution, grain shape distribution and detailed grain data obtained from laboratory observation; the other is from multi-scale tessellations. Multi-scale tessellations are realized by subdividing the cells of a primary tessellation into a secondary tessellation and combining them into one tessellation in the end. Further information about Neper's other two modules and their associated applications may be obtained from subsequent references [90–92]. This research implements Neper software to construct a GBM model that reflects grain size distribution.

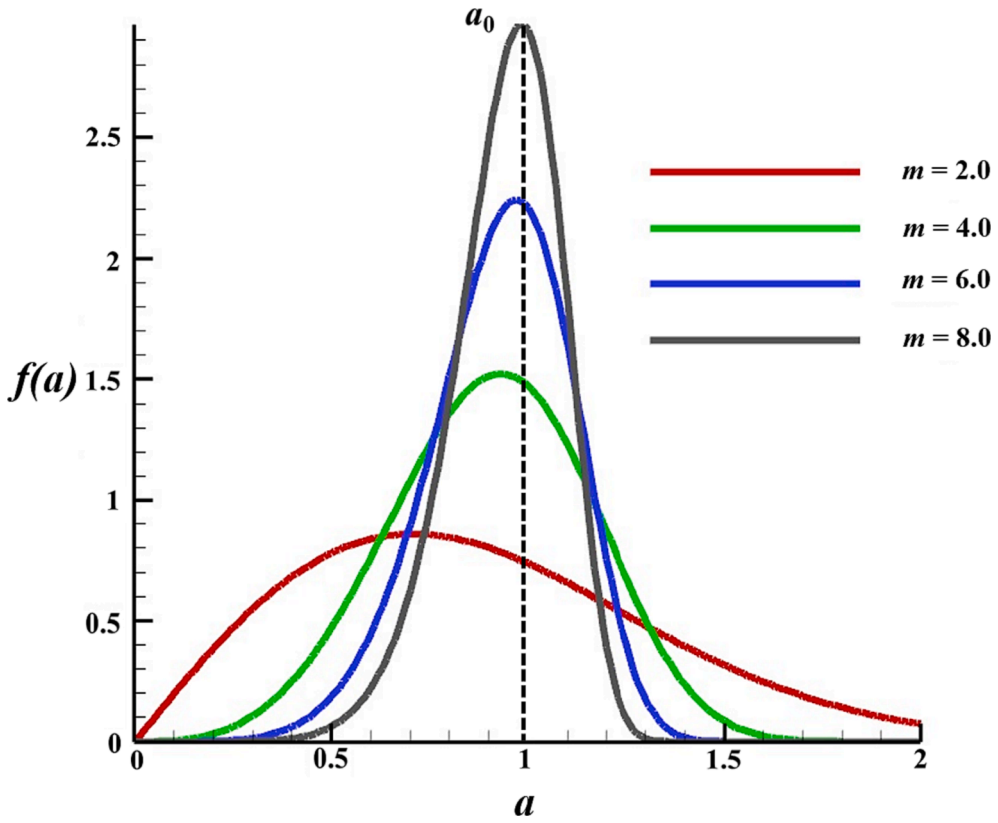

Fig. 3. Weibull distribution with different homogeneity indices.

2.6. Considering the material heterogeneity

Coal is a naturally occurring, complex, and heterogeneous geotechnical engineering material. Its mineral composition varies widely, and its properties are greatly different. The Weibull distribution function is frequently used in geotechnical engineering to evaluate the heterogeneous properties of rock and soil [93,94]. It is important to consider that the material characteristics of coal with calcite grains in a polycrystalline structure correspond to the following probability density functions, which constitute to describe its heterogeneity:

$$f(a) = \frac{m}{a}\left(\frac{a}{a_0}\right)^{m-1} \exp\left[\left(\frac{a}{a_0}\right)^{m}\right] \tag{5}$$

where:

a represents the material parameters that satisfy the distribution of the function.

a_0 is nearly equal to the average value of all material properties.

m indicates the geometric shape of the Weibull distribution function.

Fig. 3 shows the Weibull distribution function with different m values. When the value of m changes from small to large, the distribution of a tends to become more concentrated, and the shape of the Weibull distribution changes from short to high and from wide to narrow, showing that the material is more homogeneous. When $m \to \infty$, $a = a_0$, indicating that the material is completely homogeneous. Therefore, the relationship between real geometric shape and statistical distribution can be established using Eq. (5).

3. Modeling approach and parameter calibration

3.1. Model formation and boundary conditions

In this section, the Neper software is initially used to create a rectangular domain to model the behavior of the Hejiata coal sample under triaxial compression loading. The model's dimensions follow the standard of the International Society for Rock Mechanics (ISRM) [95] with a length of 100 mm and a width of 50 mm (Fig. 4(a)). The grain-growth method divides the rectangular model into tessellated regions, which are then regularized according to the predefined number of tessellation seeds. The regularization process of

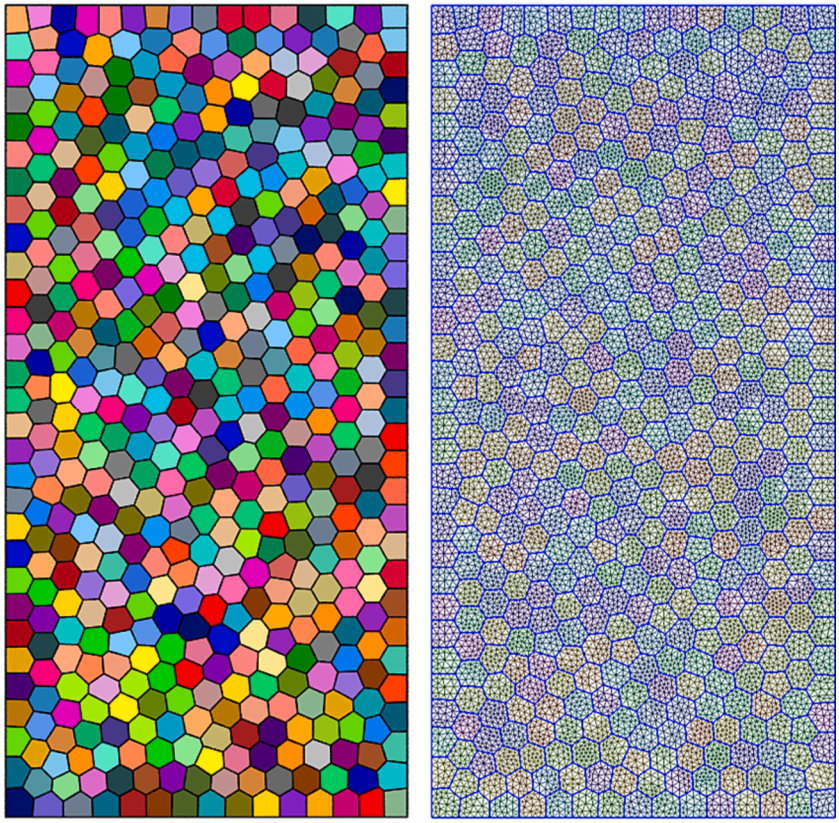

Fig. 4. Illustrate the initial model for (a) regular coal and coal with calcite grains and (b) applying to mesh.

the grain-growth method can remove all small edges, reducing the subsequent mesh's pathological behavior. The tessellated regions represent grains consisting of finer minerals, cementation, and voids, and their associated phases are randomly assigned to simulate the microstructure of Hejiata coal. Then, the generated tessellations are meshed into triangular elements (25458) with a size of 0.001 m to create a model compatible with the FDEM software MultiFracS (as seen in Fig. 4(b)). The top boundary was fixed at a constant velocity of −0.05 m/s, while the bottom boundary was fixed at a constant velocity of 0.05 m/s. The confining pressures were applied on the left and right-side boundaries at the surface force.

To study the effect of heterogeneity on mechanical properties, numerical models are generated for various homogeneity indices m = 2.0, 4.0, 6.0, and 8.0. Li et al. [36] suggest that the constructed grain size must fall within a narrow range to represent the realistic microstructures of rocks. The grain size should also be as large as possible to reduce the calculation time. Therefore, the grain number selection strategy should primarily consider the computational efficiency and running time of the model and the fact that the natural microstructure of coal with calcite grains is visible to the naked eye. As illustrated in Fig. 5, the generated two-dimensional models containing 500 Voronoi polygons are created for the triaxial compression test with various confining pressures (0.5 MPa, 1.0 MPa, 2.0 MPa, 3.5 MPa and 5.0 MPa). The numerical model with a low homogeneity index produces a more irregular grain shape distribution (Fig. 5(a and b)), and the irregularity will gradually decrease as the homogeneity index increases (Fig. 5(c and d)). For example, when the value of $m = 2.0$, the shapes of the grains are relatively narrow and sharp. However, if the value of $m = 8.0$, the grains become more rounded.

3.2. Calibration of micro parameter

Compared to the DEM, the FDEM needs the calibration of micro-parameters to simulate actual rock models precisely. However, the physical parameters in FDEM can be directly selected from those obtained in laboratory tests compared with DEM. For pure mechanical problems, only two fracture energies (Gf_I and Gf_{II}) of the joint element need to be calibrated. The basic physical parameters (density, elastic modulus, cohesion, friction angle and tensile strength, etc.) obtained by [96] the laboratory test of coal and calcite are selected as the input parameters for FDEM. Then, uniaxial and triaxial compression tests were conducted on coal and coal with calcite grains models to calibrate the fracture energies Gf_I and Gf_{II}. The triaxial compression strengths (TCS) closely match the experimental results when the values of Gf_I and Gf_{II} are set to 10 and 250 for regular coal and 10 and 200 for coal with calcite grains, as shown in Table 1. To carry out a more detailed evaluation of the effect of different homogeneity indices ($m = 2.0$, 4.0, 6.0 and 8.0), the same Gf_I and Gf_{II} values obtained from the calibration of coal with calcite grains were used. Table 2 lists the calibrated input micro parameters for the triangular and joint elements employed in the FDEM calculation.

Regular coal calibration: Firstly, the GBM model was calibrated to the Young's modulus and strength parameters (i.e., cohesion and friction angle) of regular coal models. Cohesion and friction angle were used to calibrate the GBM model and the coal's unconfined compressive strength to ensure it can capture many features of the coal under different confining pressures. Since no calcite was present in the specimens, only one set of triangular and one set of joint parameters were needed to represent the regular coal. As shown in Fig. 6, the calibration was performed using the same parameters for the coal matrix and calcite grains in the constructed GBM model. This specific model is known as the regular coal model. Confined compression tests were performed on the regular coal model with different confining pressures (0.5 MPa, 1.0 MPa, 2.0 MPa, 3.5 MPa and 5.0 MPa). The parameters were carefully modified through trial and error until Young's modulus reached a value of 2.6 GPa and peak strengths were achieved.

Coal with calcite grains calibration: Once the GBM model was calibrated to the parameters of regular coal, the parameters related

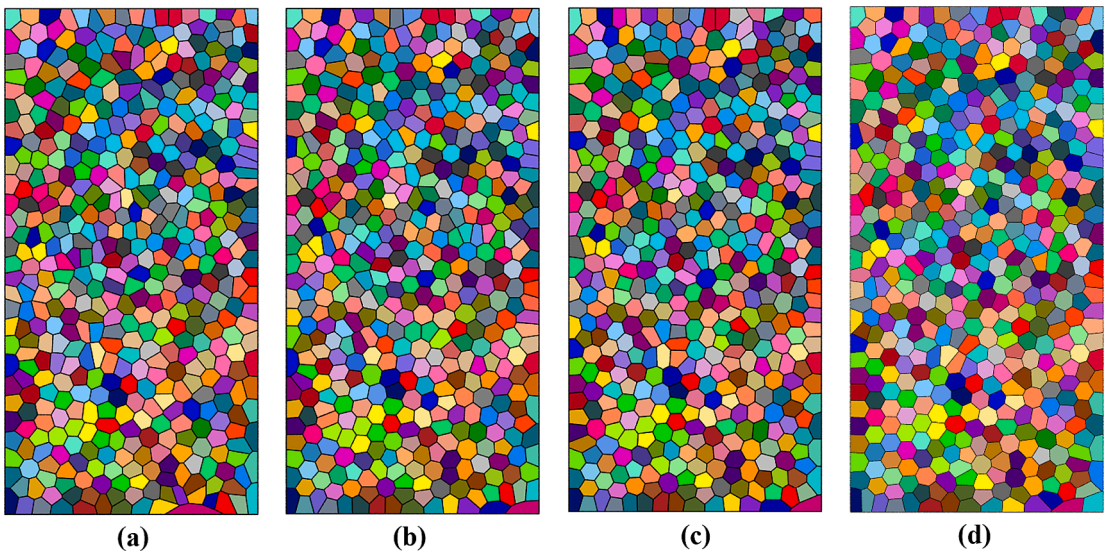

Fig. 5. Grain shape of Voronoi tessellations with different homogeneity indices (a) $m = 2.0$, (b) $m = 4.0$, (c) $m = 6.0$ and (d) $m = 8.0$.

Table 1
Calibration of Gf_{I} and Gf_{II} through Triaxial compression tests.

Confining Pressure/MPa	Regular coal Experimental Results/ MPa	Regular coal FDEM Results/ MPa	Coal with calcite grains Experimental Results/MPa	Coal with calcite grains FDEM Results/ MPa	m = 2.0	m = 4.0	m = 6.0	m = 8.0
0.5	36.4	36.3	40.2	39.6	36	39	41	43
1.0	49.5	51	42.4	45	40	42.8	45	49.8
2.0	55	57.5	51.4	52	47	48.7	52.4	56
3.5	61.4	61.7	54	56	51.7	53.4	55.8	60
5.0	64.5	64.3	56.8	60	54	56.3	60	65.3

Table 2
Input micro parameters in FDEM for simulating coal containing calcite grains and homogeneity indices.

	Triangular elements			Joint elements				
Mineral	Density/ (kg/m^3)	Elastic modulus/ (GPa)	Poisson's ratio (ν)	Cohesion/ (MPa)	Friction angle/(°)	Tensile strength/ (MPa)	Fracture energy release rate for regular coal/(J/m^2)	Fracture energy release rate for coal with calcite grains/(J/m^2)
Coal	1400	4.0	0.25	31.0	34.0	4.0	Gf_{I} = 10	Gf_{I} = 10
Calcite	2600	15.0	0.25	45.0	63.0	10.0	Gf_{II} = 250	Gf_{II} = 200
Bond	N/A	N/A	N/A	32.0	63.0	3.0		

to calcite and the bonds between calcite and coal were adjusted using the trial-and-error method. This process was carried out until the obtained Young's modulus reached a value of 3.4 GPa, and the peak strengths at various confining pressures (0.5 MPa, 1.0 MPa, 2.0 MPa, 3.5 MPa and 5.0 MPa) were achieved. Table 2 illustrates the calibrated micro parameters for both the triangular and joint elements. Fig. 7 shows a comparison between the experimentally measured strength envelope [96] and the numerically predicted strength based on the parameters assumed for the grains and bonds. It is clear from Fig. 7 that the GBM model predicted confined compressive strengths were consistent with experimental results for both the regular coal and the coal with calcite grains specimens.

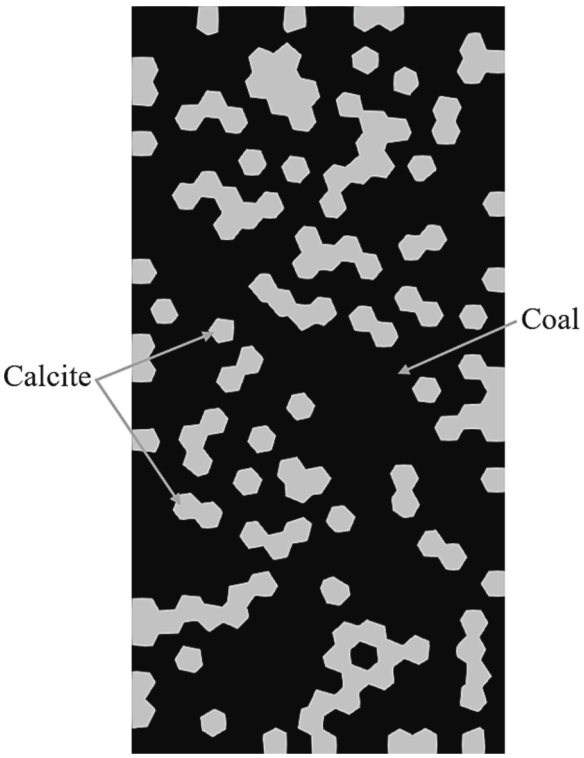

Fig. 6. Illustrate the GBM model of regular coal.

4. Results and discussion

4.1. Failure pattern

To evaluate the effect of calcite grains on the mechanical properties of coal, it is necessary to investigate the variations in the failure mechanism between regular coal, coal with calcite grains, and the homogeneity index (m) models. Fig. 8 illustrates a numerical investigation that evaluates the influence of confining pressure on the number of broken joint elements under the triaxial compression of coal and coal with calcite grains models. The important feature observed is the inverse relation between the confining pressure and the number of total, tensile and shear cracks, which show a decreasing trend of cracks as the confining pressure increases. Fig. 9 illustrates the influence of confining pressure on the number of broken joint elements Fig. 9(a) and the ratio of tensile to shear cracks Fig. 9(b). In Fig. 9(a and b), significant findings are observed where the number of broken joint elements and the ratio of tensile to shear cracks show a decreasing trend as the confining pressure increases.

Similarly, Fig. 10 illustrates the influence of heterogeneity on the development of broken joint elements in coal with calcite grains during triaxial compression. It can be seen from Fig. 10 that the number of total, tensile and shear cracks decrease with the increase of homogeneity indices m value. Fig. 11 illustrates the influence of homogeneity indices on the number of broken joint elements Fig. 11(a) and the ratio of tensile to shear cracks Fig. 11(b). As shown in Fig. 11(a and b), the number of broken joint elements and the ratio of tensile to shear cracks decrease as the homogeneity indices increase at different confining pressures. Taking a coal with calcite grains model with a homogeneity index of $m = 4.0$ as an example, it is evident that the ratio of tensile to shear cracks reduces from 2.03 % to 1.64 %, indicating a decrease of 0.39 %. This conclusion is also true for coal with calcite grains samples with different homogeneity indices ($m = 2.0$, $m = 6.0$ and $m = 8.0$).

4.2. Triaxial compression

Fig. 12 presents the axial stress-strain curves obtained from triaxial compression tests conducted on coal samples with and without calcite. The models of Hejiata coal were subjected to different confining pressures ranging from 0.5 MPa to 5.0 MPa. The results indicate that the strength of regular and coal with calcite grains increases as the confining pressures increase. However, the presence of calcite reduces the peak strength of the coal, particularly at higher confining pressures, because calcite grains cause a high degree of heterogeneity.

A more comprehensive evaluation of Fig. 12 reveals that the presence of calcite significantly improved the coal brittleness. Therefore, there is no evident brittle-to-ductile transition for the regular and coal with calcite grains models as the confining pressure increases see Fig. 12(a and b). This is because of the strong interlocking of calcite grains in the coal's post-peak behavior. When the brittle coal is loaded and peak strength is reached, the opening and slipping of fractures occur, leading to a dramatic drop in the axial stress. However, strong calcite grains significantly improve interlocking, which effectively resists fracture sliding and reduces the drop in axial stress. This interlocking effect is more prominent at high confining pressures. The numerical result is consistent with laboratory observation.

The numerical model shown in Fig. 4(a) was used again to analyze a coal with calcite grains model with various homogeneity indices. The confining pressures σ_3 were set to 0.5 MPa, 1.0 MPa, 2.0 MPa, 3.5 MPa and 5.0 MPa, whereas the associated m values were assigned as 2.0, 4.0, 6.0 and 8.0, respectively. The calculation time step was set to 5×10^{-9}sec. The input parameters for the coal with calcite grains model, such as the elastic modulus, density, cohesion, friction angle and tensile strength obtained from Fuqiang Gao, 2016 [96] and fracture energy values ($Gf_I = 10$ and $Gf_{II} = 200$) were assigned randomly using MATLAB code for the FDEM method, as

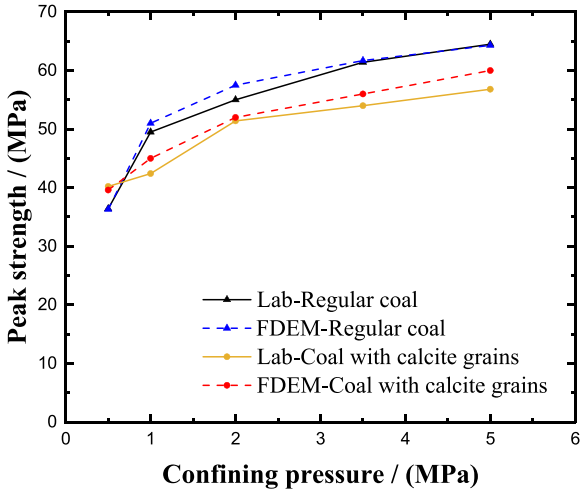

Fig. 7. Comparison of strength envelopes between experimental and numerical results.

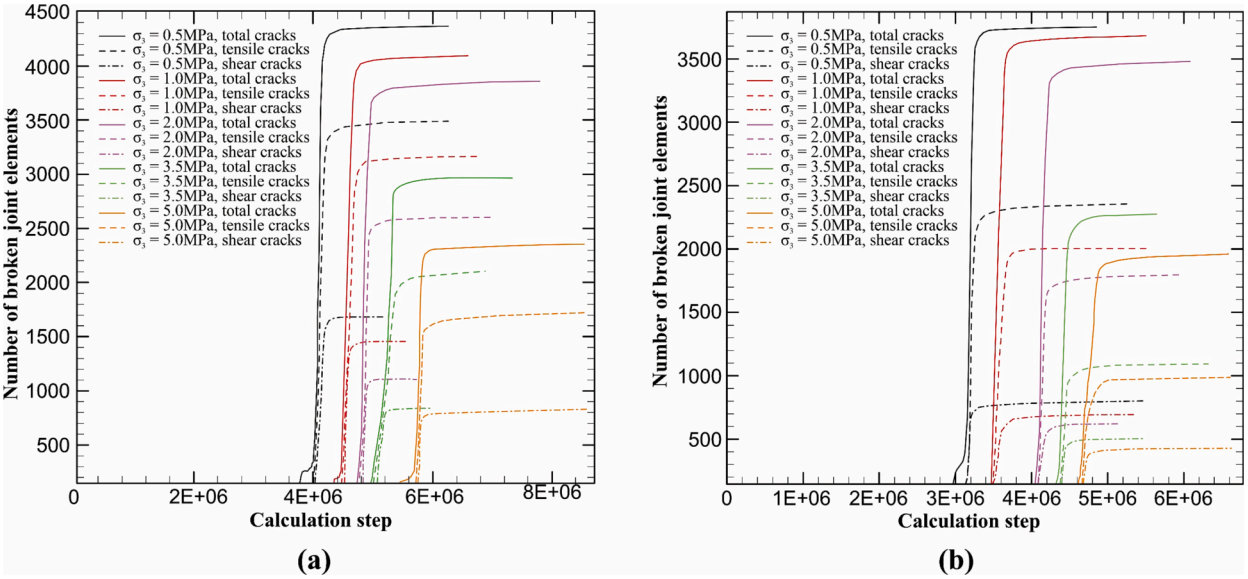

Fig. 8. Influence of different confining pressures on the number of broken joint elements for (a) regular coal model and (b) coal with calcite grains model under triaxial compression.

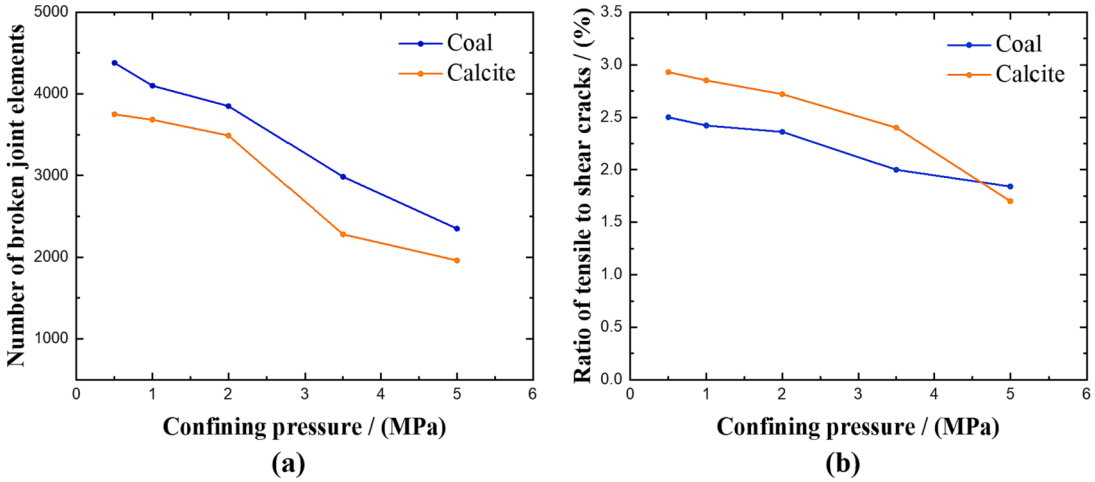

Fig.9. Influence of confining pressure on the (a) number of broken joint elements and (b) the ratio of tensile to shear cracks for regular coal and coal with calcite grains models under triaxial compression.

illustrated in Table 2. The stress-strain curves for various homogeneity indices for triaxial compression tests with different confining pressures are shown in Fig. 13. The results show that the heterogeneity has an important effect on the stress-strain curves. There is no evident brittle-to-ductile transition at constant homogeneity index and increasing confining pressure from 0.5 MPa to 5.0 MPa. The homogeneity index only influences the post-peak stage of the stress–strain curve under the triaxial compression test. The relation between the homogeneity index value and the peak value of the triaxial compressive strength is illustrated in Fig. 13, where an increase in the homogeneity index value corresponds to an increase in the peak value of the triaxial compressive strength. This finding demonstrates that a more homogeneous material exhibits greater strength during the post-peak stage, where significant deformation or failure occurs.

Hence, the following conclusions can be made:

1) For heterogeneous coal with calcite grains samples with different m values, the triaxial compressive strength σ_1 increases linearly with increasing confining pressure σ_3, as shown in Fig. 14(a).
2) However, it can be seen from Fig. 14(b) that the triaxial compressive strength σ_1 indicates an upward trend when the m values increase at the same confining pressure σ_3.

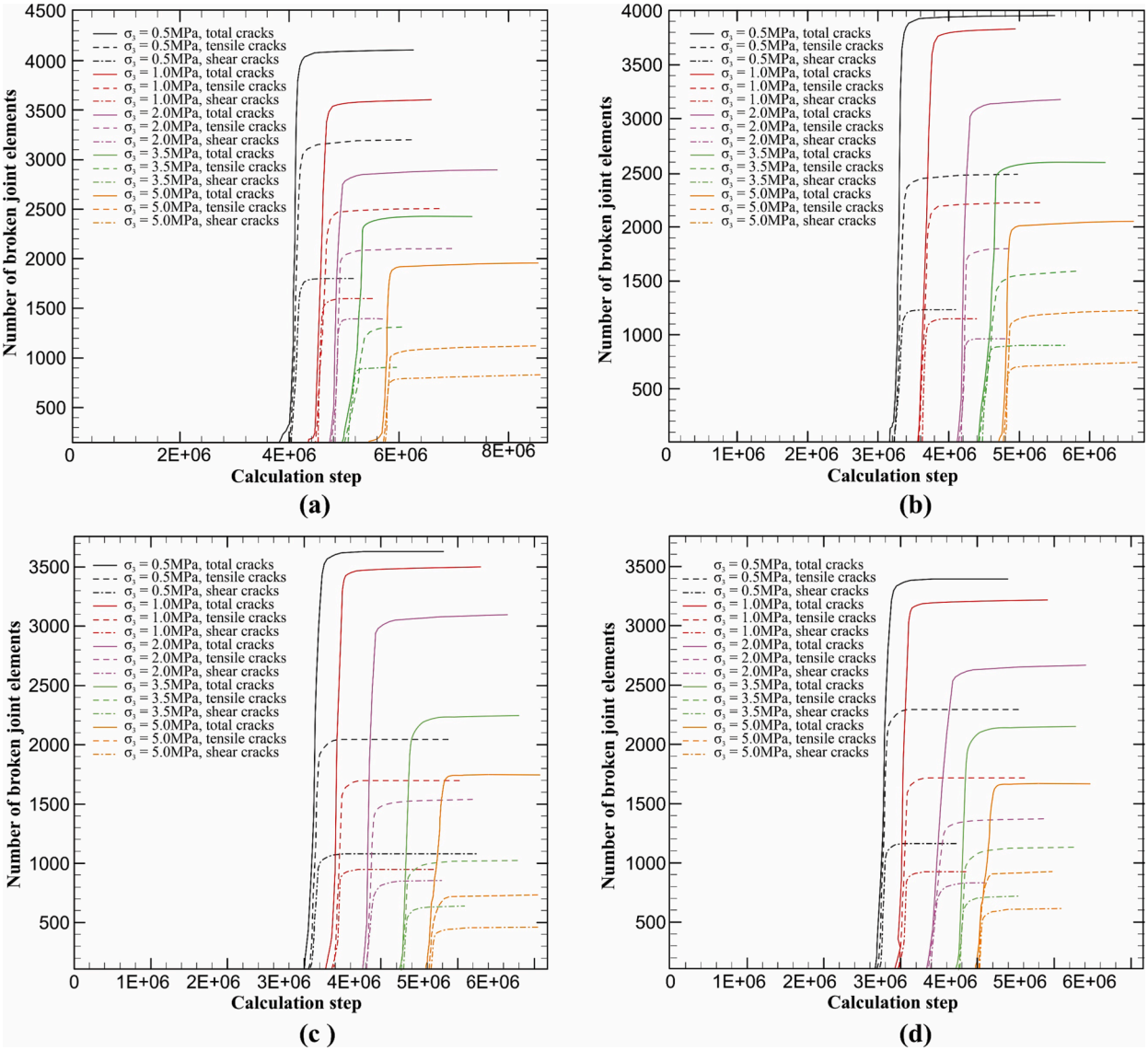

Fig. 10. Influence of heterogeneity on the number of broken joint elements for coal with calcite grains under triaxial compression (a) $m = 2.0$, (b) $m = 4.0$, (c) $m = 6.0$ and (d) $m = 8.0$.

4.3. Cracking pattern

In general, rock contains mineral grains, fractures, flaws and microcracks. For brittle rocks, the basic reason of cracking is the development of weak grain boundaries. The crack propagation occurs when the rock is loaded beyond a certain threshold. The investigation of crack initiation, propagation, and coalescence may provide valuable insights into the damage mechanisms in brittle materials. Cracks formed in the damage process can be divided into two types: tensile cracks and shear cracks. On the grain-level, cracks initiated from weak grain boundaries may extend along the grain boundaries to form inter-grain tensile and shear cracks [97]. It is also possible for cracks to propagate through the grain to form intra-grain tensile and shear cracks. The cracking patterns of the regular and coal with calcite grains models are examined at different confining pressures, as shown in Fig. 15. For regular and coal with calcite grains, as the confining pressure increases, the failure pattern shows a trend from tensile failure to shear failure. A large number of shear failures represented by red color occur in regular and coal with calcite grains models when subjected to a confining pressure of 0.5 MPa. The ratio of shear cracks increases when the confining pressure increases from 0.5 MPa to 5.0 MPa. However, the prevalence of tensile failure represented by blue color remains prominent, as shown in Fig. 15(a and b).

The failure modes of the generated model for various homogeneity indices ($m = 2.0$, $m = 4.0$, $m = 6.0$ and $m = 8.0$) in triaxial compression tests with different confining pressures are shown in Fig. 16. Under triaxial compression, the homogeneity index significantly affects the failure mode. For instance, if the homogeneity index is low (e.g., $m = 2.0$), more elongated and sharp-angled

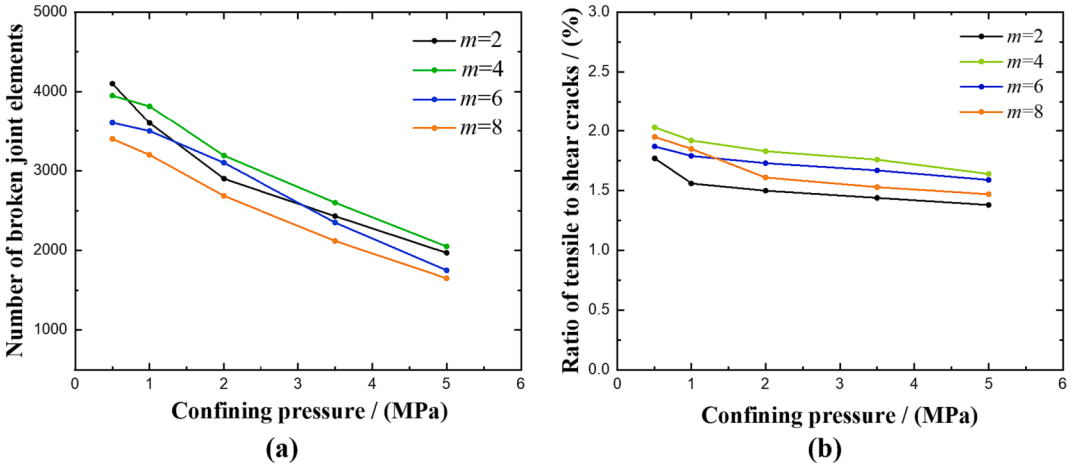

Fig. 11. Influence of heterogeneity on the (a) number of broken joint elements and (b) the ratio of tensile to shear cracks for coal with calcite grains under triaxial compression.

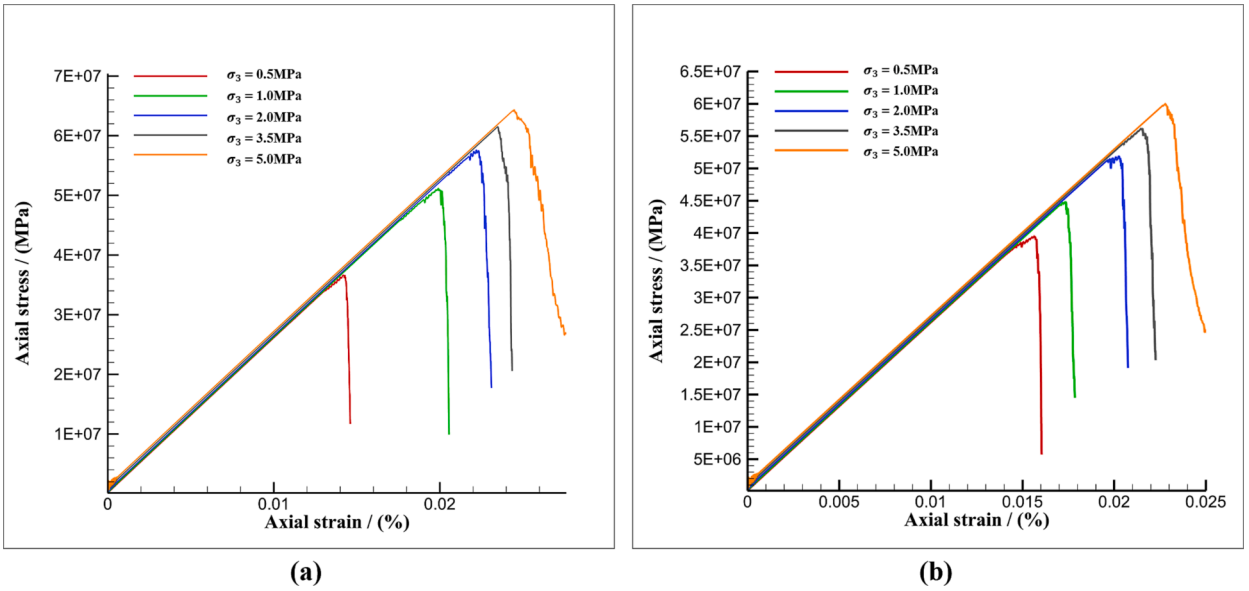

Fig. 12. Axial stress-strain curves for (a) regular coal and (b) coal with calcite grains.

polygonal grains are generated in the numerical model. Cracks generated in this geometric microstructure are distributed more evenly. As pointed out by Eberhardt et al. [98], this type of geometric structure contributes to providing preferred and continuous paths of weakness for growing microcracks to propagate along and promote a more rapid coalescence and interaction of grain boundary and intra-grain cracks. When the homogeneity index is high, such as $m = 8.0$, the numerical specimen shows a higher formation of convex polygonal grains. The failure mechanism of numerical models has approximately perpendicular orientation to the horizontal direction. After that, cracks propagate more sparsely in a numerical model, resulting in the development of a splitting failure. Therefore, splitting failure occurs along the boundaries of different homogeneity index models, specifically in the center, left, and right-side boundaries.

5. Conclusions

A grain-based model is an efficient and valuable simulation strategy for analyzing the mechanical properties of crystalline solid materials. In the present research, grain structures are generated in Neper software using a normal distribution of grains and then imported into MultiFracS to describe the deformation behavior. A comprehensive parametric study has been carried out by using the laboratory results of regular coal and coal with calcite grains. Based on the parametric study results, calibration procedures are used to determine the mechanical parameters of coal containing calcite grains. This study employed the finite-discrete element method (FDEM) to investigate the effect of calcite grains on the mechanical properties of coal. The homogeneity index is utilized in the Weibull

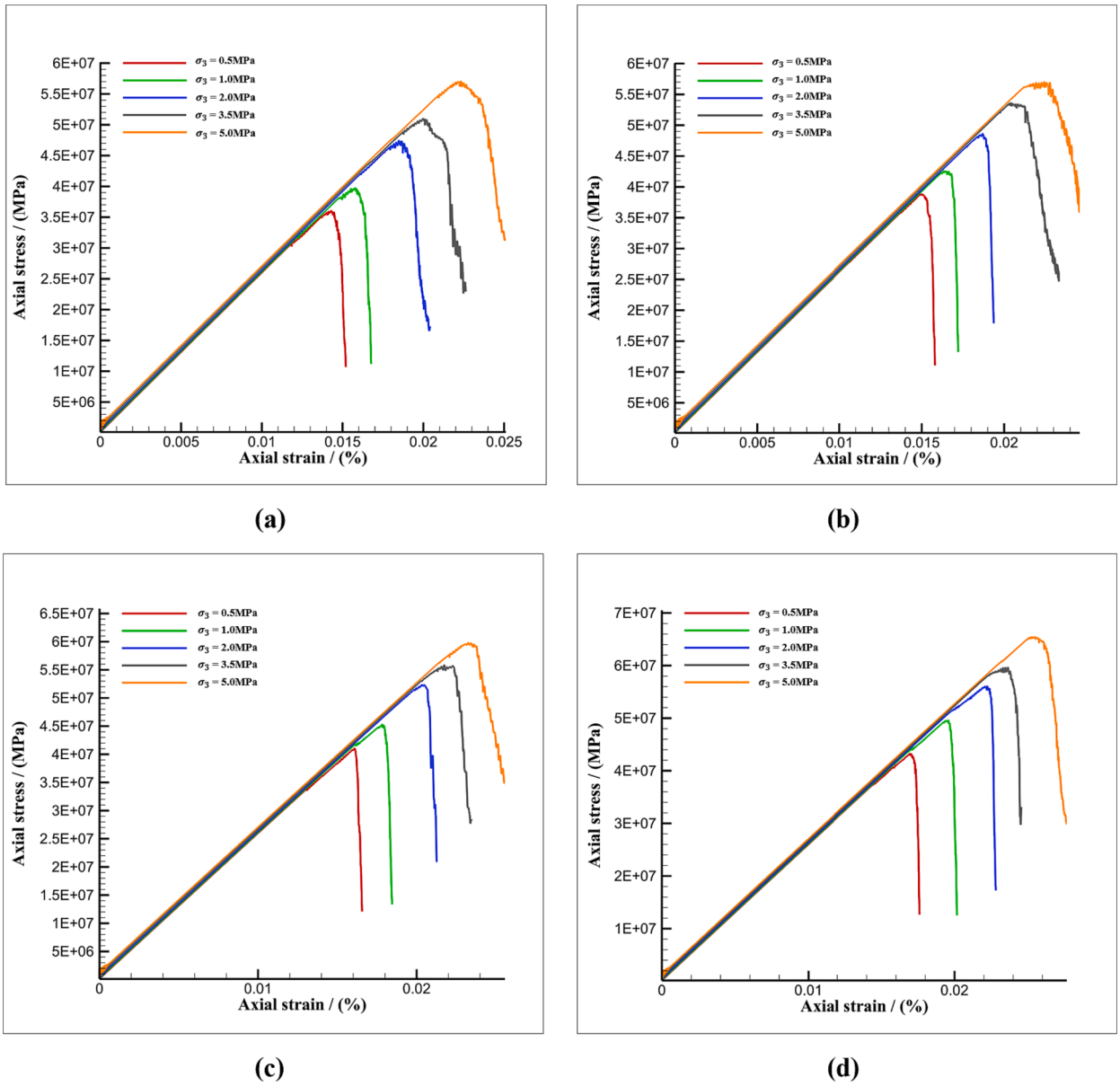

Fig. 13. Stress–strain curves for different homogeneity indices (a) $m = 2.0$, (b) $m = 4.0$, (c) $m = 6.0$ and (d) $m = 8.0$.

statistical distribution and is integrated into MultiFracS to determine the material heterogeneity resulting from the geometric microstructure. The proposed GBM model can accurately represent the actual microstructure of coal with calcite grains and provide a quantitative investigation of the influence of heterogeneity on mechanical properties by conducting triaxial compression tests. The following conclusions can be drawn:

1) The presence of calcite increases the Young's modulus of coal from 2.6 to 3.4 GPa.
2) Calcite reduces the peak strength of coal, particularly at high confining pressures.
3) The number of broken joint elements and the ratio of tensile to shear cracks decrease as the confining pressure increases.
4) Heterogeneity has a significant influence on the stress-strain curves under confined compression tests and it is found that the triaxial compressive strength increases linearly with the heterogeneity m value.
5) The influence of microstructural heterogeneity significantly affects the cracking behavior associated with the corresponding failure mechanisms. Many cracks are distributed throughout the numerical model at low heterogeneity, while at high heterogeneity, cracks are distributed more sparsely.

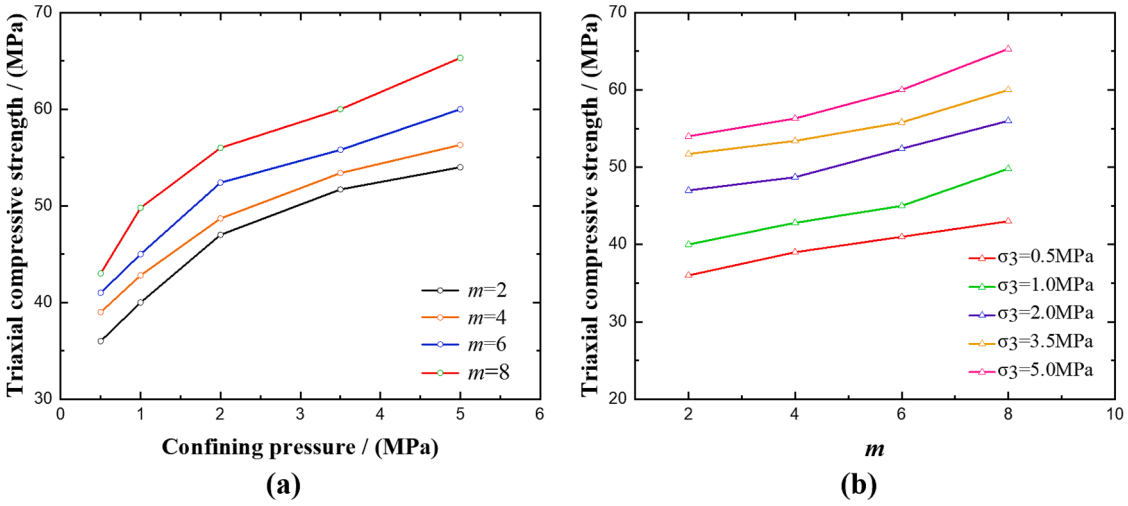

Fig. 14. Triaxial compressive strength of various confining pressures and *m* values (a) and (b) are the different presentation forms.

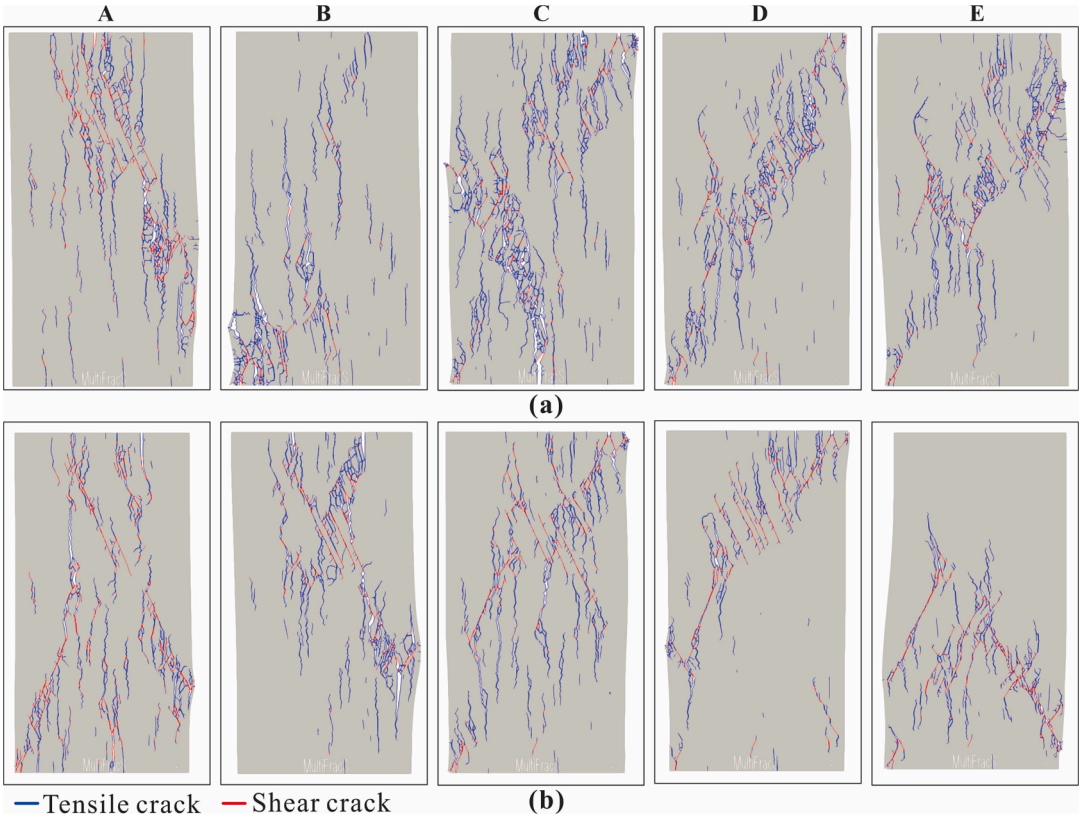

Fig. 15. Cracking patterns of the (a) regular coal and (b) coal with calcite grains under confined compression with different confining pressures of (A) 0.5 MPa, (B) 1.0 MPa, (C) 2.0 MPa, (D) 3.5 MPa and (E) 5.0 MPa.

CRediT authorship contribution statement

Sajid Ali: Writing – original draft, Visualization, Investigation, Formal analysis, Data curation. **Chengzeng Yan:** Writing – review & editing, Software, Methodology, Funding acquisition. **Tie Wang:** Writing – review & editing, Formal analysis, Data curation. **Yuchen Zheng:** Formal analysis, Data curation. **Du Han:** Formal analysis, Data curation. **Wenhui Ke:** Formal analysis, Data curation.

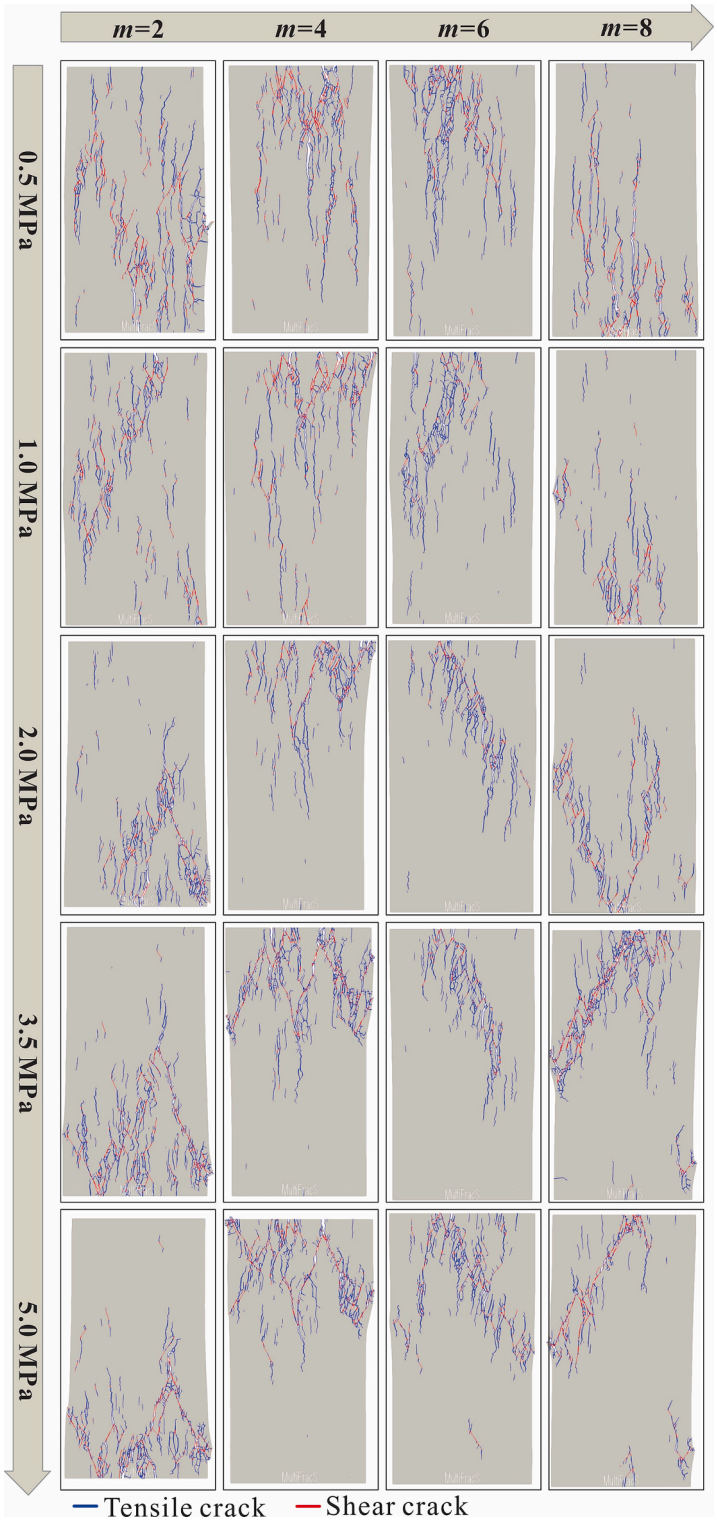

Fig. 16. Failure patterns of numerical models with different homogeneity indices through compressive tests with various confining pressures.

Declaration of competing interest

The authors declare that they have no known competing financial interests or personal relationships that could have appeared to influence the work reported in this paper.

Data availability

Data will be made available on request.

Acknowledgments

This work was supported by State Key Laboratory of Intelligent Construction and Healthy Operation and Maintenance of Deep Underground Engineering (SKLGDUEK2206).

References

[1] Chen J, Liu P, Zhao H, Zhang C, Zhang J. Analytical studying the axial performance of fully encapsulated rock bolts. Eng Fail Anal 2021;128:105580.
[2] Tang J-Z, Yang S-Q, Tian W-L, Tao Y. Effect of confining pressure on mechanics and deformation behavior of sandstone containing a single inclined joint. Eur J Environ Civ Eng 2022;26(3):1022–45.
[3] Vazaios I, Vlachopoulos N, Diederichs MS. Assessing fracturing mechanisms and evolution of excavation damaged zone of tunnels in interlocked rock masses at high stresses using a finite-discrete element approach. J Rock Mech Geotech Eng 2019;11(4):701–22.
[4] Xiao TL, Huang M, Li XP. Research on strength and deformation with marble of deep rock mass considering confining pressure effect. Chin J Under Spa Eng 2018;14(02):362–8.
[5] Yao Q, Wang W, Zhu L, Xia Z, Tang C, Wang X. Effects of moisture conditions on mechanical properties and AE and IR characteristics in coal–rock combinations. Arab J Geosci 2020;13:1–15.
[6] Dawson GKW, Golding SD, Esterle JS, Massarotto P. Occurrence of minerals within fractures and matrix of selected Bowen and Ruhr Basin coals. Int J Coal Geol 2012;94:150–66.
[7] Karacan CÖ, Okandan E. Fracture/cleat analysis of coals from Zonguldak Basin (northwestern Turkey) relative to the potential of coalbed methane production. Int J Coal Geol 2000;44(2):109–25.
[8] Karacan CÖ. Swelling-induced volumetric strains internal to a stressed coal associated with CO2 sorption. Int J Coal Geol 2007;72(3–4):209–20.
[9] Karacan CÖ, Mitchell GD. Behavior and effect of different coal microlithotypes during gas transport for carbon dioxide sequestration into coal seams. Int J Coal Geol 2003;53(4):201–17.
[10] Cutruneo CMNL, et al. A mineralogical and geochemical study of three Brazilian coal cleaning rejects: demonstration of electron beam applications. Int J Coal Geol 2014;130:33–52.
[11] Dai S, Ren D, Ma S. The cause of endemic fluorosis in western Guizhou Province, Southwest China. Fuel 2004;83(14–15):2095–8.
[12] Huggins FE, Seidu LBA, Shah N, Backus J, Huffman GP, Honaker RQ. Mobility of elements in long-term leaching tests on Illinois# 6 coal rejects. Int J coal Geol 2012;94:326–36.
[13] al Cho N, Martin CD, Sego DC. A clumped particle model for rock. Int J rock Mech Min Sci 2007;44(7):997–1010.
[14] Tan X, Konietzky H, Chen W. Numerical simulation of heterogeneous rock using discrete element model based on digital image processing. Rock Mech Rock Eng 2016;49:4957–64.
[15] Abdelaziz A, Zhao Q, Grasselli G. Grain based modelling of rocks using the combined finite-discrete element method. Comput Geotech 2018;103:73–81.
[16] Li C-S, Zhang D, Du S-S, Shi B. Computed tomography based numerical simulation for triaxial test of soil–rock mixture. Comput Geotech 2016;73:179–88.
[17] Liu G, Cai M, Huang M. Mechanical properties of brittle rock governed by micro-geometric heterogeneity. Comput Geotech 2018;104:358–72.
[18] Mahabadi OK, Tatone BSA, Grasselli G. Influence of microscale heterogeneity and microstructure on the tensile behavior of crystalline rocks. J Geophys Res Solid Earth 2014;119(7):5324–41.
[19] Manouchehrian A, Cai M. Influence of material heterogeneity on failure intensity in unstable rock failure. Comput Geotech 2016;71:237–46.
[20] Peng J, Wong LNY, Teh CI. Influence of grain size heterogeneity on strength and microcracking behavior of crystalline rocks. J Geophys Res Solid Earth 2017;122(2):1054–73.
[21] D. O. Potyondy. "A grain-based model for rock: approaching the true microstructure." *Proc. rock Mech. Nord. Ctries.* 9–12. 2010.
[22] Zhang Y, Wong LNY, Chan KK. An extended grain-based model accounting for microstructures in rock deformation. J Geophys Res Solid Earth 2019;124(1):125–48.
[23] J. D. Frost and S. McNeil. "Imaging technologies: Techniques and applications in civil engineering." 1998.
[24] Frost JD, Wright JR. Digital Image Processing, American Society of Civil Engineers. New York: NY, USA; 1993.
[25] Xu W, Yue Z, Hu R. Study on the mesostructure and mesomechanical characteristics of the soil–rock mixture using digital image processing based finite element method. Int J Rock Mech Min Sci 2008;45(5):749–62.
[26] Chen S, Yue ZQ, Tham LG. Digital image-based numerical modeling method for prediction of inhomogeneous rock failure. Int J rock Mech Min Sci 2004;41(6):939–57.
[27] Tang CA, Liu H, Lee PKK, Tsui Y, Tham Lg. Numerical studies of the influence of microstructure on rock failure in uniaxial compression—part I: effect of heterogeneity. Int J Rock Mech Min Sci 2000;37(4):555–69.
[28] Tang CA, Tham LG, Wang SH, Liu H, Li WH. A numerical study of the influence of heterogeneity on the strength characterization of rock under uniaxial tension. Mech Mater 2007;39(4):326–39.
[29] Gao F, Stead D, Elmo D. Numerical simulation of microstructure of brittle rock using a grain-breakable distinct element grain-based model. Comput Geotech 2016;78:203–17.
[30] Hofmann H, Babadagli T, Yoon JS, Zang A, Zimmermann G. A grain based modeling study of mineralogical factors affecting strength, elastic behavior and micro fracture development during compression tests in granites. Eng Fract Mech 2015;147:261–75.
[31] Lan H, Martin CD, Hu B. Effect of heterogeneity of brittle rock on micromechanical extensile behavior during compression loading. J Geophys Res Solid Earth 2010;115(B1):pp.
[32] Wong LNY, Peng J, Teh CI. Numerical investigation of mineralogical composition effect on strength and micro-cracking behavior of crystalline rocks. J Nat Gas Sci Eng 2018;53:191–203.
[33] Yoon JS, Zang A, Stephansson O. Simulating fracture and friction of Aue granite under confined asymmetric compressive test using clumped particle model. Int J Rock Mech Min Sci 2012;49:68–83.
[34] Zhou J, Lan H, Zhang L, Yang D, Song J, Wang S. Novel grain-based model for simulation of brittle failure of Alxa porphyritic granite. Eng Geol 2019;251:100–14.
[35] N. Bahrani, D. Potyondy, and M. Pierce. "Simulation of Brazilian test using PFC2D grain-based model," in *Proceedings of 21st Canadian rock mechanics symposium, Edmonton*. 2012.

[36] Li XF, Li HB, Zhao J. 3D polycrystalline discrete element method (3PDEM) for simulation of crack initiation and propagation in granular rock. Comput Geotech 2017;90:96–112.
[37] Liu N, Li M, Chen W. Mechanical deterioration of rock salt at different confinement levels: A grain-based lattice scheme assessment. Comput Geotech 2017;84:210–24.
[38] Bathe K. "Finite element method", Wiley Encycl. Comput Sci Eng 2007:1–12.
[39] Moghadam SN, Nazokkar K, Chalaturnyk RJ, Mirzabozorg H. Parametric assessment of salt cavern performance using a creep model describing dilatancy and failure. Int J Rock Mech Min Sci 2015;79:250–67.
[40] Wang T, Yang C, Chen J, Daemen JJK. Geomechanical investigation of roof failure of China's first gas storage salt cavern. Eng Geol 2018;243:59–69.
[41] Xing W, Zhao J, Hou Z, Were P, Li M, Wang G. Horizontal natural gas caverns in thin-bedded rock salt formations. Environ Earth Sci 2015;73:6973–85.
[42] Yang Y, Sun G, Zheng H, Qi Y. Investigation of the sequential excavation of a soil-rock-mixture slope using the numerical manifold method. Eng Geol 2019;256:93–109.
[43] Bahrani N, Kaiser PK. Numerical investigation of the influence of specimen size on the unconfined strength of defected rocks. Comput Geotech 2016;77:56–67.
[44] Hu M, Zhang B, Li B, Cao W. Using Discrete Element Method to Study the Rock Breaking Effect of Worn TBM Cutters. Geotech Geol Eng 2022;40(5):2843–56.
[45] Xia H, Wu A, Lu B, Xu D. Influence mechanism of heterogeneity on mechanical properties of rock materials. J Yangtze River Sci Res Inst 2021;38(3):103.
[46] Lei Z, Rougier E, Euser B, Munjiza A. A smooth contact algorithm for the combined finite discrete element method. Comput Part Mech 2020;7:807–21.
[47] Lisjak A, Liu Q, Zhao Q, Mahabadi OK, Grasselli G. Numerical simulation of acoustic emission in brittle rocks by two-dimensional finite-discrete element analysis. Geophys J Int 2013;195(1):423–43.
[48] Mohammadnejad T, Khoei AR. Hydro-mechanical modeling of cohesive crack propagation in multiphase porous media using the extended finite element method. Int J Numer Anal Methods Geomech 2013;37(10):1247–79.
[49] Munjiza A, Knight EE, Rougier E. Large strain finite element method: a practical course. John Wiley & Sons; 2015.
[50] Munjiza AA, Knight EE, Rougier E. Computational mechanics of discontinua. John Wiley & Sons; 2011.
[51] Rougier E, Knight EE, Broome ST, Sussman AJ, Munjiza A. Validation of a three-dimensional finite-discrete element method using experimental results of the split Hopkinson pressure bar test. Int J rock Mech Min Sci 2014;70:101–8.
[52] Sun L, Liu Q, Tao S, Grasselli G. A novel low-temperature thermo-mechanical coupling model for frost cracking simulation using the finite-discrete element method. Comput Geotech 2022;152:105045.
[53] Cao W, Younis R M. Empirical scaling of formation fracturing by high-energy impulsive mechanical loads. International Journal of Rock Mechanics and Mining Sciences 2024;173:105613.
[54] Yan C, Zheng Y, Wang G. A 2D adaptive finite-discrete element method for simulating fracture and fragmentation in geomaterials. Int. J. Rock Mech. Min. Sci. 2023;169:105439.
[55] Yan C, Jiao Y-Y, Zheng H. A fully coupled three-dimensional hydro-mechanical finite discrete element approach with real porous seepage for simulating 3D hydraulic fracturing. Comput Geotech 2018;96:73–89.
[56] Yan C, Jiao Y-Y, Yang S. A 2D coupled hydro-thermal model for the combined finite-discrete element method. Acta Geotech 2019;14:403–16.
[57] Yan C, Luo Z, Zheng Y, Ke W. A 2D discrete moisture diffusion model for simulating desiccation fracturing of soil. Eng Anal Bound Elem 2022;138:42–64.
[58] Yan C, Wang Y, Xie X, et al. A 2D continuous-discrete mixed seepage model considering the fluid exchange and the pore pressure discontinuity across the fracture for simulating fluid-driven fracturing[J]. Acta Geotechnica 2023;18(11):5791–810.
[59] Yan C, Ma H, Tang Z, et al. A two-dimensional moisture diffusion continuous model for simulating dry shrinkage and cracking of soil[J]. *Int. J. Geotech*, 2022, 22(10): 04022172.
[60] Yan C, Guo H, Tang Z. Three-dimensional continuous-discrete pore-fracture mixed seepage model and hydro-mechanical coupling model to simulate hydraulic fracturing[J]. Journal of Petroleum Science and Engineering, 2022, 215: 110510.
[61] Yan C, Ren Y, Yang Y. A 3D thermal cracking model for rockbased on the combined finite–discrete element method. Comput. Part. Mech. 2020;(7):881–901.
[62] Yan C, Gao Y, Guo H A FDEM. Based 3D discrete mixed seepage model for simulating fluid driven fracturing. Eng. Anal. Bound. Elem. 2022;140:447–63.
[63] Yan CZ, Zheng H. A new potential function for the calculation of contact forces in the combined finite–discrete element method. Int. J. Numer. Anal. methods Geomech. 2017;41:265–83.
[64] Yan C., Jiao, Y. FDEM-TH3D: A three-dimensional coupled hydrothermal model for fractured rock. *Int. J. Numer. Anal. Methods Geomech.* **2019**, *43*, 415–440.
[65] Yan C, Xie X, Ren Y, Ke W, Wang G. A FDEM-Based 2D coupled thermal-hydro-mechanical model for multiphysical simulation of rock fracturing. Int. J. Rock Mech. Min. Sci. 2022;149:104964.
[66] Yan C, Wang T, Gao Y, et al. A three-dimensional grouting model considering hydromechanical coupling based on the combined finite-discrete element method. *Int. J. Geotech*, 2022, 22(11): 04022189.
[67] Yan C, Wei D, Wang G. Three-dimensional finite discrete element-based contact heat transfer model considering thermal cracking in continuous–discontinuous media. Computer Methods in Applied Mechanics and Engineering 2022;388:114228.
[68] Yan C, Tong Y, Luo Z, et al. A two-dimensional grouting model considering hydromechanical coupling and fracturing for fractured rock mass. Engineering Analysis with Boundary Elements 2021;133:385–97.
[69] Yan C, Zheng Y, Ke W, et al. A FDEM 3D moisture migration-fracture model for simulation of soil shrinkage and desiccation cracking. Computers and Geotechnics 2021;140:104425.
[70] Yan C, Wang T, Ke W, et al. A 2D FDEM-based moisture diffusion–fracture coupling model for simulating soil desiccation cracking. Acta Geotechnica 2021;16:2609–28.
[71] Yan C, Wang X, Huang D, et al. A new 3D continuous-discontinuous heat conduction model and coupled thermomechanical model for simulating the thermal cracking of brittle materials. International Journal of Solids and Structures 2021;229:111123.
[72] Yan C, Fan H, Huang D, et al. A 2D mixed fracture–pore seepage model and hydromechanical coupling for fractured porous media. Acta Geotechnica 2021;16(10):3061–86.
[73] Yan C, Yang Y, Wang G. A new 2D continuous-discontinuous heat conduction model for modeling heat transfer and thermal cracking in quasi-brittle materials. Computers and Geotechnics 2021;137:104231.
[74] Yan C, Zheng Y, Huang D, et al. A coupled contact heat transfer and thermal cracking model for discontinuous and granular media. Computer Methods in Applied Mechanics and Engineering 2021;375:113587.
[75] Yan C, Jiao Y Y. A 2D discrete heat transfer model considering the thermal resistance effect of fractures for simulating the thermal cracking of brittle materials. Acta Geotechnica 2020;15:1303–19.
[76] Yan C, Jiao Y Y, Zheng H. A three-dimensional heat transfer and thermal cracking model considering the effect of cracks on heat transfer. International Journal for Numerical and Analytical Methods in Geomechanics 2019;43(10):1825–53.
[77] Yan C, Zheng H. Three-dimensional hydromechanical model of hydraulic fracturing with arbitrarily discrete fracture networks using finite-discrete element method. International Journal of Geomechanics 2017;17(6):04016133.
[78] Yan C, Jiao Y Y. A 2D fully coupled hydro-mechanical finite-discrete element model with real pore seepage for simulating the deformation and fracture of porous medium driven by fluid. Computers & Structures 2018;196:311–26.
[79] Yan C, Zheng H. A two-dimensional coupled hydro-mechanical finite-discrete model considering porous media flow for simulating hydraulic fracturing. International Journal of Rock Mechanics and Mining Sciences 2016;88:115–28.
[80] Yan C, Zheng H, Sun G, et al. Combined finite-discrete element method for simulation of hydraulic fracturing. Rock mechanics and rock engineering 2016;49:1389–410.
[81] Yan C, Zheng H. FDEM-flow3D: A 3D hydro-mechanical coupled model considering the pore seepage of rock matrix for simulating three-dimensional hydraulic fracturing. Computers and Geotechnics, 2017, 81: 212-228.

[82] Zheng Y, Yan C, Zheng H. Modified joint element constitutive model for FDEM to simulate the nonlinear mechanical behavior of rocks. Computers and Geotechnics 2023;164:105831.
[83] Yan C, Zhao Z, Yang Y, Zheng H. A three-dimensional thermal-hydro-mechanical coupling model for simulation of fracturing driven by multiphysics. Comput Geotech 2023;155:105162.
[84] Munjiza A, Andrews KRF, White JK. Combined single and smeared crack model in combined finite-discrete element analysis. Int J Numer Methods Eng 1999;44 (1):41–57.
[85] Munjiza A, Owen DRJ, Bicanic N. A combined finite-discrete element method in transient dynamics of fracturing solids. Eng Comput 1995.
[86] Munjiza AA. The combined finite-discrete element method. John Wiley & Sons; 2004.
[87] Yan C, Zheng H. A coupled thermo-mechanical model based on the combined finite-discrete element method for simulating thermal cracking of rock. Int J Rock Mech Min Sci 2017;91:170–8.
[88] Munjiza A, Andrews KRF. NBS contact detection algorithm for bodies of similar size. Int J Numer Methods Eng 1998;43(1):131–49.
[89] Munjiza A, Andrews KRF. Penalty function method for combined finite–discrete element systems comprising large number of separate bodies. Int J Numer Methods Eng 2000;49(11):1377–96.
[90] Quey R, Dawson PR, Barbe F. Large-scale 3D random polycrystals for the finite element method: Generation, meshing and remeshing. Comput Methods Appl Mech Eng 2011;200(17–20):1729–45.
[91] Barbe F, Quey R. A numerical modelling of 3D polycrystal-to-polycrystal diffusive phase transformations involving crystal plasticity. Int J Plast 2011;27(6): 823–40.
[92] Quey R, Renversade L. Optimal polyhedral description of 3D polycrystals: Method and application to statistical and synchrotron X-ray diffraction data. Comput Methods Appl Mech Eng 2018;330:308–33.
[93] Fang Z, Harrison JP. Development of a local degradation approach to the modelling of brittle fracture in heterogeneous rocks. Int J Rock Mech Min Sci 2002;39 (4):443–57.
[94] Tang S, Yu C, Tang C. Numerical modeling of the time-dependent development of the damage zone around a tunnel under high humidity conditions. Tunn Undergr Sp Technol 2018;76:48–63.
[95] E. T. Brown, "The ISRM Suggested Methods for Rock Characterization, Testing and Monitoring: 2007–2014, R. Ulusay (Ed.) Springer International Publishing, Cham, Switzerland (2015), p. 293,(83.29€. ISBN 978-3-319-07712-3 (Hbk), 978-3-319-07713-0 (eBook))." Elsevier. 2015.
[96] Gao F, Kang H, Wu Y. Experimental and numerical study on the effect of calcite on the mechanical behaviour of coal. Int J Coal Geol 2016;158:119–28.
[97] Wang T, Yan C. Investigating the influence of water on swelling deformation and mechanical behavior of mudstone considering water softening effect. Eng Geol 2023;318:107102.
[98] Eberhardt E, Stimpson B, Stead D. Effects of grain size on the initiation and propagation thresholds of stress-induced brittle fractures. Rock Mech rock Eng 1999; 32:81–99.